Challenges and opportunities in quantitative brain PET imaging

Lopes Alves, Isadora

6

Parametric imaging of [^{11}C]flumazenil binding in the rat brain

Author(s): *Isadora Lopes Alves*, David Vállez García, Andrea Parente, Janine Doorduin, Ana Maria Marques da Silva, Michel Koole, Rudi Dierckx, Antoon Willemsen, Ronald Boellaard

Under review by the Journal of Molecular Imaging and Biology

Introduction

The *in vivo* study of neuronal integrity has been well established by means of Positron Emission Tomography (PET) imaging with [^{11}C]flumazenil[1,2]. A number of different conditions have previously been studied with [^{11}C]flumazenil[3–5], and the link between the GABA-ergic system and neurological disorders[6] and inflammation[7] has increased the applicability and interest in PET imaging with this radiotracer.

In addition to the non-invasive character of PET, one of its main advantages for studying physiological processes is that it can provide quantitative information. Full quantitative analysis can be achieved by pharmacokinetic modeling, which describes the time course of the PET tracer in tissue and enables the estimation of different parameters related to tracer distribution, metabolism, or receptor density and binding[8,9]. In that context, the quantification of [^{11}C]flumazenil binding has been previously performed by different pharmacokinetic models. In human studies, the one tissue compartment model (1TCM) and the simplified reference tissue model (SRTM)[10] using the pons as a reference tissue have been validated[11] and applied[12–14]. Although useful, these models have been mostly applied for regional quantification of [^{11}C]flumazenil binding, analyzing the average kinetic profile of a specific volume of interest (VOI).

In cases when subtle or disease-specific changes are expected, VOI-based pharmacokinetic modeling might be suboptimal precisely due to the use of pre-defined volumes of interest (VOIs). If physiological changes are restricted to a subset of a region (tissue heterogeneity) or if they do not follow anatomical delineations, the average signal from pre-defined VOIs might not be able to properly describe the underlying alterations. There, the generation and analysis of parametric images can be of greater use. Parametric images are graphical representations of quantitative endpoints, where every image voxel corresponds to a kinetic parameter, such as distribution volume (V_T) or binding potential (BP_{ND}). Although parametric imaging is most commonly applied to human studies, it could be of great interest for the analysis of animal PET data. Preclinical PET imaging plays an important role in drug development and treatment assessment studies, for example, and it could be advantageous to explore full kinetic analysis of subtle physiological changes by parametric imaging also in the

context of such animal study designs. Moreover, parametric imaging enables group comparisons at the voxel level using statistical parametric mapping (SPM), which performs the statistical analysis independent of pre-defined regions of interest.

In human studies, parametric images of [^{11}C]flumazenil binding have been generated from a number of different methods, and the Logan graphical analysis, a multilinear reference tissue model (MRTM2), and the receptor parametric mapping method (RPM) were found to provide the best quantitative metrics[15]. However, no similar analysis has been performed for animal data. Moreover, the preference and performance of VOI-based models have already been shown to differ between human and rat studies[16]. Together with the higher noise levels typical of animal PET data, this difference could indicate the parametric models found to work best for the analysis of human studies might not be the most appropriate in the pre-clinical setting.

The aim of the current study was, therefore, to investigate the performance of several parametric methods for the analysis of [^{11}C]flumazenil PET images of the rat brain. To that end, we retrospectively analyzed [^{11}C]flumazenil pre-clinical images with both plasma input and reference tissue based parametric methods, and compared the results to their corresponding VOI-based pharmacokinetic models.

Material and Methods

Animal data

We retrospectively analyzed male Wistar-Unilever outbred rats (n=10) obtained from Harlan (Horst, The Netherlands). The animal experiments were performed according to the Dutch Law on Animal Experiments and were approved by the Institutional Animal Care and Use Committee of the University of Groningen (6264B).

Data acquisition

Prior to the PET scan, a mixture of 5% isoflurane and medical air was used to anesthetize the animals, which were maintained under anesthesia at 1.5-2.0%, with a flow of 1.5-2ml/min. Scans were performed in the Focus 220 camera (Siemens Medical Solutions, USA), where

animals were positioned trans-axially with the head in the field of view. First, a transmission scan was performed with a point-source of ^{57}Co. Next, [^{11}C]flumazenil was injected (bolus injection) with an automatic pump over 60s and the PET camera was started at the moment of injection. List-mode PET data was acquired for a period of 60min.

During the scan, arterial blood samples (0.1ml) were obtained (n=16) for each individual animal. The samples were subsequently separated into blood and plasma and the activity was measured in a gamma counter (LKB-Wallac, Finland). For the metabolite analysis, 2-3 larger samples (0.6ml) were collected for a number of animals and a population metabolite curve was constructed by combining data from the individual samples. Finally, this curve was used for the construction of individual metabolite corrected plasma input functions.

Image processing

After all necessary corrections, the list-mode data was reconstructed into 21 frames (6×10, 4×30, 2×60, 1×120, 1×180, 4×300 and 3×600s). The 2D-OSEM algorithm was used to reconstruct the Fourier rebinned sinograms, with 4 iterations and 16 subsets. The resulting images displayed a 128×128×95 matrix, 0.63mm pixel width and 0.79mm slice thickness. Next, individual dynamic images were coregistered to a [^{11}C]flumazenil template[17] in PMOD v3.7 (PMOD Technologies Ltd., Switzerland). Time-activity curves (TACs) were then generated from a set of pre-defined bilateral volumes of interest (VOIs) which included the whole brain, regions with high $GABA_A$ expression (frontal cortex and hippocampus), and regions with low $GABA_A$ expression (cerebellum, medulla and pons). Following previous studies[16], the pons was set as the pseudo-reference tissue and its TAC was used as input for reference based models. In order to minimize bias induced by noise in the parametric methods, an isotropic 3D Gaussian filter (FWHM = 0.8mm) was applied.

Pharmacokinetic modeling

All pharmacokinetic modeling was performed with the PPET[18] software package.

First, parametric distribution volume (V_T) images were generated from three different methods, including the Basis Function Method (BFM), which is an implementation of the one tissue compartment model (1TCM), the Logan Graphical Analysis (Logan) and the Spectral

Analysis (SA)[19]. For these methods, the metabolite corrected plasma curve was used as input function. Next, parametric binding potential (BP_{ND}) images were computed from three reference based models. The first was the Reference Tissue Logan Graphical Analysis (RLogan), which provides the distribution volume ratio (DVR) of target regions relative to the reference tissue. Following the relationship $BP_{ND} = DVR - 1$[8], we subtracted 1 from the RLogan DVR to allow direct comparison to parametric images of BP_{ND}. The other two methods consisted of two implementations of the receptor parametric mapping method (RPM, SRTM2)[20], which correspond to the two versions of the simplified reference tissue model (SRTM and SRTM2). For the SRTM2, the model fit was performed in two steps, where the median value of the reference tissue efflux rate constant (k_2') obtained in the first run was entered as a fixed parameter for the second run[21]. An overview of the settings used for the parametric methods can be found in Table 1.

Table 1. Overview of settings for parametric methods

Method		start t (min)	end t (min)	basis start t (min)	basis end t (min)	# basis functions
V_T	**BFM**	-	-	0.00083	0.016	50
	Logan	10	60	-	-	
	SA	-	-	0.00333	0.333	30
SUV	**SUV_{30-40}**	30	40	-	-	
	SUV_{40-50}	40	50	-	-	
	SUV_{50-60}	50	60	-	-	
BP_{ND}	**RLogan**	10	60	-	-	
	RPM	-	-	0.01	0.2	50
	SRTM2	-	-	0.01	0.2	50
	$SUVR_{30-40} - 1$	30	40	-	-	
	$SUVR_{40-50} - 1$	40	50	-	-	
	$SUVR_{50-60} - 1$	50	60	-	-	

Parametric images of Standardized Uptake Value (SUV) and SUV target to pons ratio (SUVR) were also generated for the intervals 30min-40min, 40min-50min and 50min-60min post-injection (p.i.) and subsequently referred to by $SUV_{start-end}$ and $SUVR_{start-end}$. In order to

compare SUVR and BP_{ND} images, 1 was subtracted from the derived SUVR values, assuming equilibrium was reached for those intervals.

Method evaluation

Results from each of the parametric methods were compared to 1) the corresponding regional (VOI) analysis using equivalent kinetic models, but also to 2) reference values based on regional 2TCM fits. The 2TCM derived parameters (V_T and DVR – 1) were considered as reference values for method comparison. An overview of parametric methods, their corresponding VOI-models, parameter of interest and equivalent 2TCM parameter can be found in Table 2.

For that purpose, first the same pre-defined set of VOIs used for the generation of TACs were projected onto the parametric images and average parameter estimates were obtained for each region. Next, the regional TACs were analyzed by six models corresponding to the parametric methods (i.e., 1TCM, Logan, SA, RLogan, SRTM and SRTM2), as well as by the 2TCM. Finally, the regionally averaged values from parametric methods were compared to both their VOI-counterparts, as well as to the corresponding 2TCM-derived reference.

Table 2. Overview of VOI-based and parametric methods and their corresponding quantitative parameters

VOI	Parametric	Parameter of interest	Additional parameter	Reference parameter
1TCM	BFM	V_T	-	2TCM V_T
Logan	Logan	V_T	-	2TCM V_T
SA	SA	V_T	K_1 and model order	2TCM V_T
-	SUV	SUV	-	2TCM V_T
RLogan	RLogan	DVR	-	2TCM DVR – 1
SRTM	RPM	BP_{ND}	R_1	2TCM DVR – 1
SRTM2	SRTM2	BP_{ND}	R_1	2TCM DVR – 1
-	SUVR	SUVR	-	2TCM DVR – 1

Statistical analysis

Parameter agreement was assessed by linear regression analysis and Bland-Altman plots. Results were considered significant when $p<0.05$, and are expressed as mean ± SD.

Results

Volume of distribution (V_T)

Visual inspection of parametric V_T images showed good correspondence between methods, as well as the expected [^{11}C]flumazenil distribution in the rat brain (Figure 1).

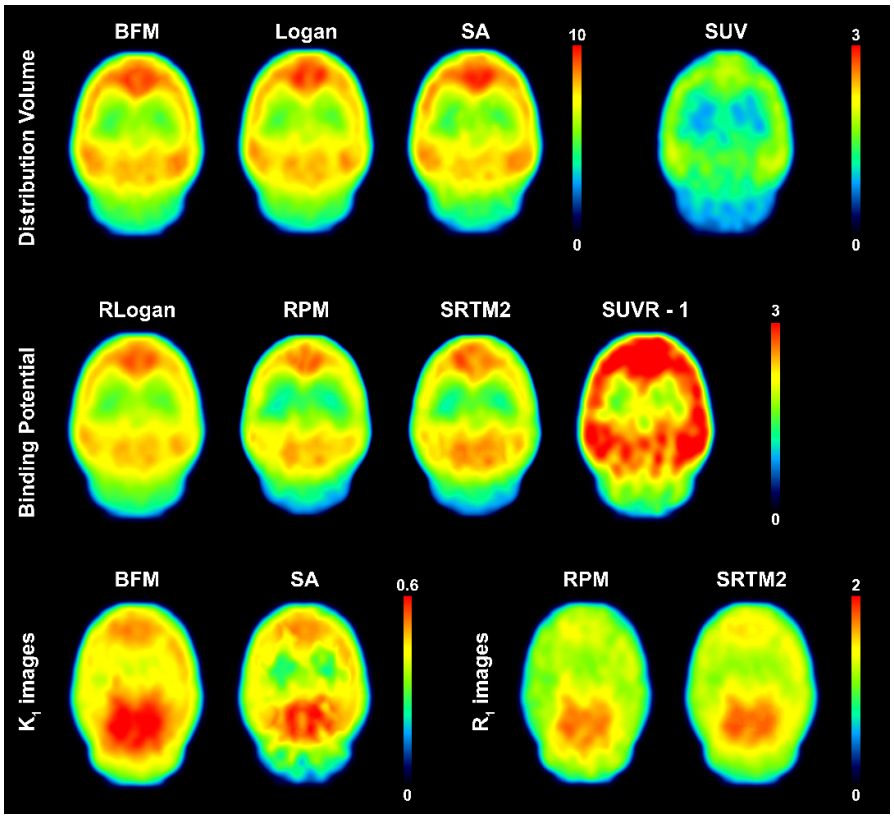

Figure 1. Representative (n=1) parametric images of V_T (top left corner), SUV_{30-40} (top right corner), BP_{ND} (middle section), K_1 images (bottom left corner) and R_1 images (bottom right corner).

Compared to their VOI-counterpart, parametric Logan was the method with the best correlation, displaying an R^2=0.99 and a slope of 0.97 when the regression line was set through the origin (Table 3). The BFM also strongly correlated to its counterpart (1TCM) values (R^2=0.98), with a slope of 1.03. The slope of the linear regression of SA with its counterpart was further from identity (0.89), and the correlation was somewhat lower than the other methods

(R^2=0.96). Overall, all three methods showed excellent correlation (R^2=0.99) to 2TCM reference V_T values (Figure 2A). However, BFM was the method which displayed the slope closest to the identity line (0.98). Although SA showed the same correlation coefficient as the other two methods, a slope of 0.93 indicated a larger underestimation in V_T values.

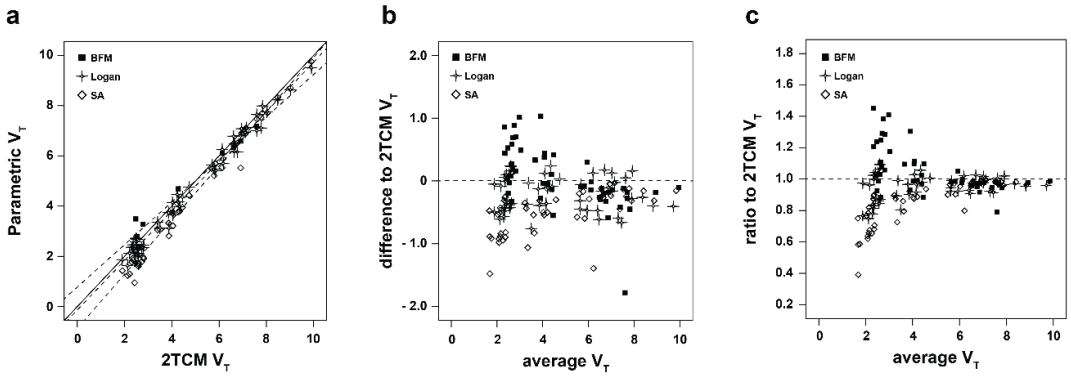

Figure 2. Regression analysis and Bland-Altman plots of V_T compared to 2TCM values. **(A)** Linear regression between parametric (BFM, Logan, SA) and 2TCM V_T values determined by VOI analysis. The solid line is the identity line, and the dashed lines represent the regression lines. **(B)** Bland-Altman plot of the agreement in V_T estimation between the parametric methods and the reference values obtained from the 2TCM (VOI). The dashed line represents zero bias. **(C)** Ratio Bland-Altman plot between BFM, Logan and SA, and 2TCM V_T values. The dashed line represents a ratio of one, corresponding to full agreement between methods.

Table 3. Linear regression analysis between parametric methods and their VOI-counterparts, as well as between parametric and reference values from 2TCM (VOI). Linear regression analysis was performed with and without setting the intercept to zero (through origin columns).

	VOI-counterpart					VOI-2TCM				
Model	R^2	slope	Int.	R^2 (through origin)	slope (through origin)	R^2	slope	int.	R^2 (through origin)	slope (through origin)
V_T										
BFM	0.96	0.79	1.35	0.98	1.03	0.96	0.85	0.78	0.99	0.98
Logan	0.99	1.03	-0.35	0.99	0.97	0.98	0.98	-0.13	0.99	0.96
SA	0.85	0.94	-0.28	0.96	0.89	0.98	1.08	-0.87	0.99	0.93
SUV_{30-40}	-	-	-	-	-	0.87	0.27	-0.16	0.96	0.24
SUV_{40-50}	-	-	-	-	-	0.87	0.21	-0.15	0.96	0.18
SUV_{50-60}	-	-	-	-	-	0.83	0.16	-0.09	0.95	0.14
BP_{ND}										
RLogan	0.99	1.03	-0.10	0.99	0.97	0.98	0.92	-0.10	0.99	0.86
RPM	0.98	1.15	-0.09	0.99	1.08	0.97	0.98	-0.82	0.98	0.93
SRTM2	0.95	1.32	-0.63	0.97	0.91	0.97	0.89	0.15	0.98	0.98
$SUVR_{30-40} - 1$	-	-	-	-	-	0.98	1.21	-0.14	0.99	1.13
$SUVR_{40-50} - 1$	-	-	-	-	-	0.97	1.30	-0.16	0.98	1.21
$SUVR_{50-60} - 1$	-	-	-	-	-	0.94	1.17	-0.17	0.96	1.07

The Bland-Altman analysis showed that, despite the good correlation, a negative bias (-0.20) was present with the Logan method (Figure 2B). The BFM had the smallest overall bias in relation to 2TCM V_T (0.05); yet, its 95% limits of agreement were slightly wider than those of Logan (Table 4). SA had the widest 95% limits of agreement similar to BFM and an overall higher (negative) bias (-0.49). Figure 2C shows a ratio Bland-Altman plot to highlight the performance in parameter agreement for the different levels of V_T values. There, regions with high V_T (≥6) had a ratio close to one in comparison with 2TCM V_T values. On the other hand, larger over- and underestimations occurred for regions of lower V_T (<6).

Table 4. Bland Altman analysis of agreement between parametric and VOI-counterpart methods, as well as between parametric and 2TCM (VOI) values.

		VOI-counterpart		VOI-2TCM	
Parameter	**Method**	**bias**	**95% L. A.**	**bias**	**95% L. A.**
V_T					
	BFM	0.44	-0.79 to 1.67	0.05	-0.89 to 1.00
	Logan	-0.20	-0.57 to 0.17	-0.19	-0.74 to 0.34
	SA	-0.57	-2.42 to 1.27	-0.49	-1.16 to 0.18
BP_{ND}					
	RLogan	-0.07	-0.21 to 0.06	-0.17	-0.41 to 0.05
	RPM	0.03	-0.28 to 0.34	-0.10	-0.37 to 0.16
	SRTM2	-0.22	-0.74 to 0.29	0.05	-0.27 to 0.38
	$SUVR_{30-40} - 1$	-	-	0.05	-0.37 to 0.49
	$SUVR_{40-50} - 1$	-	-	0.13	-0.51 to 0.77
	$SUVR_{50-60} - 1$	-	-	-0.01	-0.59 to 0.58

Figure 3 displays the range of differences to 2TCM values for the three parametric methods across all regions. Significant differences in bias were found in all three methods when compared to 2TCM values. However, the bias from parametric Logan compared to 2TCM values showed the smallest variability (SD=0.19), indicating higher precision for this method compared to the others.

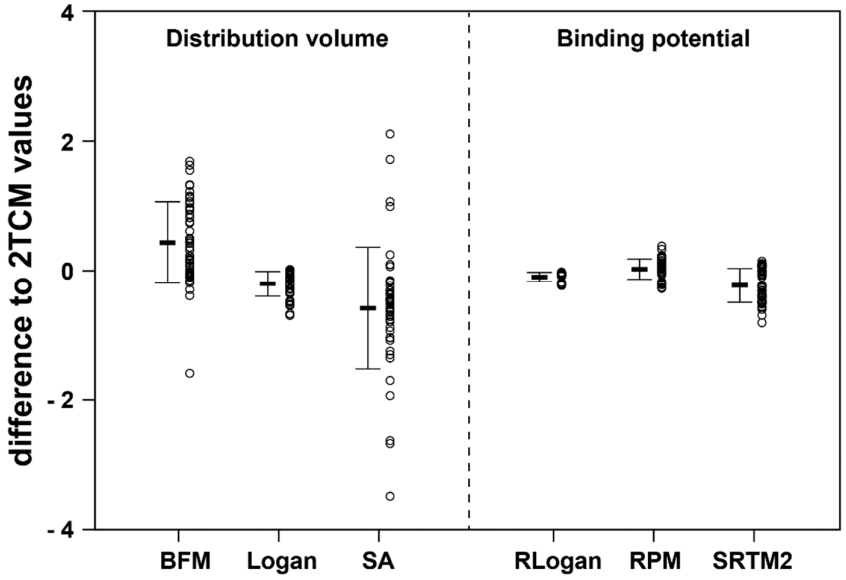

Figure 3. Plot of differences in estimates between each parametric method and 2TCM reference values across regions. Individual values are represented by circles, the mean is represented by the black line and the bars represent the SD.

Binding potential (BP_{ND} and DVR – 1)

As can be seen in Figure 1, the highest [^{11}C]flumazenil binding spatially matched regions with a high receptor density (cortical and sub-cortical areas), while the lowest was seen in low-density ones (cerebellum and brainstem). Images of receptor binding were also visually comparable between parametric methods.

All reference based methods performed well in comparison to 2TCM DVR – 1 (Figure 4A). In particular, DVR – 1 from RLogan displayed the best correlation coefficient in relation to 2TCM values (R^2=0.99), while the slope was the furthest from the identity line (0.86), indicating underestimation of receptor binding. Binding estimates from RPM showed correlation to 2TCM values similar to those of RLogan(R^2=0.98), and a slope closer to identity (0.93) (Table 3). Estimation of binding from parametric SRTM2 outperformed both other methods in terms of linear regression, with a R^2 of 0.98 and a slope of 0.98 compared to 2TCM values.

Bland-Altman plots indicated a similar performance between RLogan and RPM methods (Figure 4B). Both parametric methods displayed a negative bias compared to 2TCM DVR – 1 (-0.17 for RLogan and -0.10 for RPM). SRTM2 showed a small overall bias (0.05), but resulted in the largest 95% limits of agreement to 2TCM DVR – 1, as can be seen in Table 4. For most levels of specific binding, all three methods showed good relative agreement, with a ratio close to one in comparison with 2TCM DVR – 1 values (Figure 4C). However, relative errors were larger for BP_{ND} values close to zero.

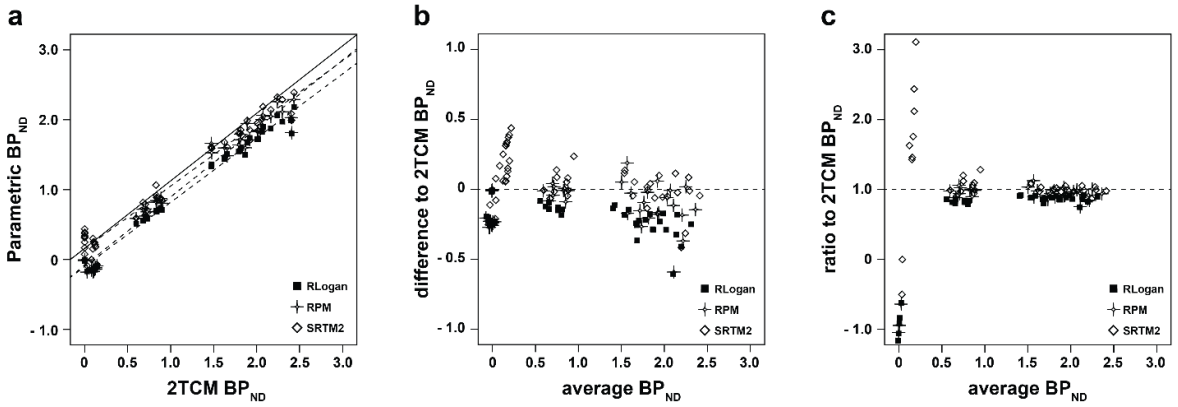

Figure 4. Regression analysis and Bland-Altman plots of BP_{ND}. **(A)** Linear regression between parametric (RLogan, RPM, SRTM2) and 2TCM DVR – 1 (BP_{ND}) values determined by VOI analysis. The solid line represents the identity line, and the dashed lines correspond to each of the regression lines. **(B)** Bland-Altman plot of the agreement in BP_{ND} estimation between the parametric methods and the reference values obtained from the 2TCM (VOI). The dashed line corresponds to zero bias. **(C)** Ratio Bland-Altman plot between BP_{ND} of parametric methods and 2TCM BP_{ND}. The dashed line corresponds to a ratio of one, representing full agreement between methods. The y-axis is truncated at -1.0.

In Figure 3, a similar performance between the reference methods can be seen. Significant differences were found in the bias of parametric RLogan and SRTM2 when compared to 2TCM values. No significant difference was seen for the RPM bias to 2TCM values ($p=0.20$). Yet, RLogan displayed the highest precision (SD=0.72) compared to the other two methods.

SUV and SUVR – 1

Correlation between parametric SUV and 2TCM V_T was overall strong, with similar correlation coefficients across intervals p.i. (R^2=0.96, R^2=0.96 and R^2=0.95 for SUV_{30-40}, SUV_{40-50} and SUV_{50-60} respectively). However, there was a clear scale difference between the two parameters, and a direct comparison was not possible, as SUV ranged from 0.2 to 2.7 and 2TCM V_T ranged from 1.9 to 9.9 (Figure 5A). However, ratio Bland-Altman plots showed that SUV from all three intervals underestimated 2TCM V_T in a similar manner across regions, independent of the levels of uptake (Figure 5B).

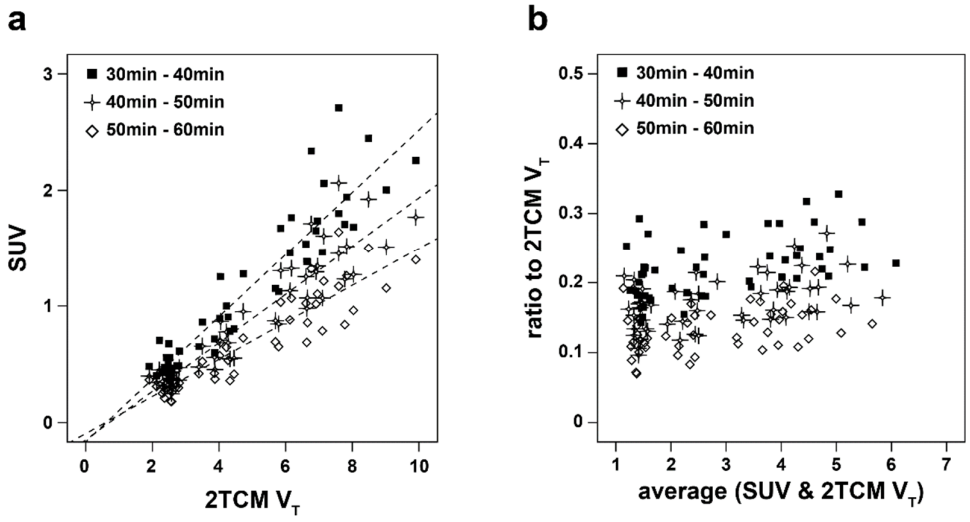

Figure 5. Regression analysis and ratio Bland-Altman plot of SUV from different intervals. **(A)** Regression analysis between SUV (parametric) and 2TCM V_T (VOI) for three different intervals p.i. The dashed lines represent the regression lines. **(B)** Ratio Bland-Altman plot between V_T estimates from SUV and from 2TCM V_T (VOI) for the same intervals.

SUVR – 1 images showed excellent correlation to binding estimates from 2TCM for all intervals p.i. (Figure 6A). However, an overestimation of binding potential from SUVR – 1 images was seen, with linear regression (through origin) slopes of 1.13, 1.21 and 1.07 for the $SUVR_{30-40}$ – 1, $SUVR_{40-50}$ – 1, and $SUVR_{50-60}$ – 1, respectively. This was confirmed by a Bland-Altman analysis, where SUVR40-50 – 1 showed the highest bias compared to 2TCM DVR – 1, as well as the largest 95% limits of agreement (Table 4). In a ratio Bland-Altman, all intervals

show similar performance, with the ratio close to one for most levels of specific binding (Figure 6B). For binding values close to zero, relative errors were more pronounced, independent of the SUVR interval.

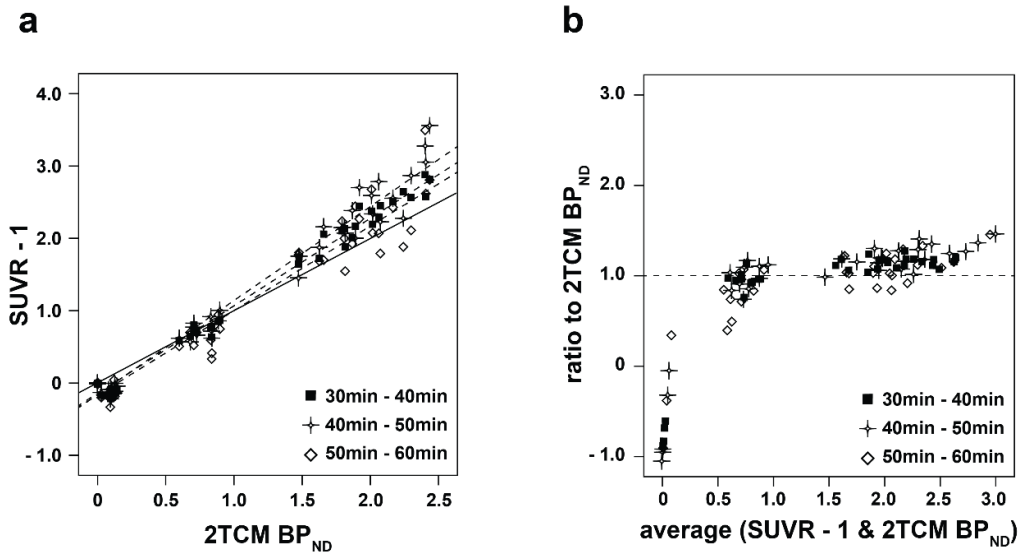

Figure 6. Regression analysis and ratio Bland-Altman plot of SUVR from different intervals. **(A)** Regression analysis between SUVR – 1 (parametric) and 2TCM BP_{ND} (VOI) for three different p.i. intervals. The solid line represents the identity line and the dashed lines correspond to each of the regression lines. **(B)** Ratio Bland-Altman plot between binding potential estimates from SUVR – 1 and from 2TCM BP_{ND} (VOI) for the same intervals. The dashed line corresponds to a ratio of one, representing full agreement between methods. The y-axis is truncated at -1.0.

Parametric images of K_1, R_1 and model order

For BFM and SA, parametric images of K_1 (influx rate constant) were also available (Figure 1). Although both displayed similar perfusion, BFM K_1 was generally higher, while the less homogeneous distribution seen in the SA image suggested higher noise sensitivity for that method. SA also provided parametric images of model order, displaying the difference in the complexity of kinetic profiles between different voxels (Figure 7). In those, a marked difference between high- and low-density regions is seen, and a more complex model was more frequently observed in the later, compared to the former.

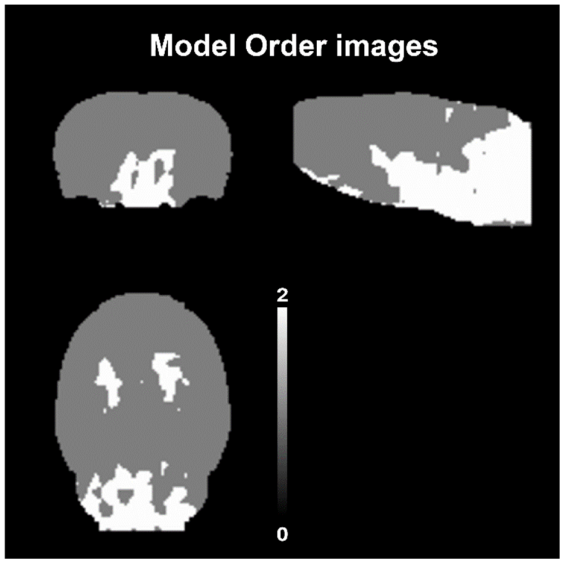

Figure 7. Representative image (n=1) of model order obtained from the parametric SA method, displaying, in the different views, a difference between cortical and non-cortical regions.

Additional parametric images were also available from RPM and SRTM2 displaying R_1, i.e., the ratio between K_1 of a target region and of the pseudo-reference tissue (pons). As can be seen in Figure 1, there is a good correspondence between the two methods. However, R_1 images from SRTM2 displayed better contrast and lower noise levels compared to RPM R_1 images.

Discussion

The use of parametric imaging methods for the analysis of PET data can be of importance when subtle and/or disease-specific changes are expected. In the case of [^{11}C]flumazenil brain PET, those changes are related to the GABA-ergic system and can be present in several conditions related to neuronal loss and inflammatory processes. While parametric images of [^{11}C]flumazenil distribution and binding have been generated and applied in human studies, the same has not yet been done for the pre-clinical setting. Therefore, this study evaluated several parametric methods for the visualization and analysis of [^{11}C]flumazenil PET images of the rat brain.

A first analysis of parametric V_T images demonstrated that all three methods tested in this study (BFM, Logan and SA) corresponded well to their VOI-counterparts. These results

indicate that the generation of parametric V_T maps from these methods could, to some extent, replicate results obtained from a regional analysis, which is generally less affected by noise and image resolution. More importantly, there was also an excellent correlation between parametric values of each of the three parametric methods and V_T estimated from the reference 2TCM VOI analysis. In terms of parameter agreement, however, a slight difference between the methods becomes noticeable. While BFM V_T showed a small bias compared to 2TCM values (0.05), the wide 95% limits of agreement suggest this method might not be optimal for parameter estimation at the individual level. A similar behavior could be seen with V_T estimates from SA. This variability was especially true for regions of small V_T (low-density regions), where an absolute difference in the range of ±1 corresponds to a relative bias of approximately 40% (see Figure 2B and 2C). This observation is in agreement with a previous report of a VOI analysis, where we found the difference between 1TCM and 2TCM V_T values to be larger for cerebellum, medulla and pons[16]. On the other hand, such a range of differences might not be relevant for most study designs, as regions with low-density of receptors are generally not the main focus of an analysis. Nonetheless, even though this region-dependent range of agreement was seen in all three methods, the range of differences to 2TCM values was smallest for Logan, as can be graphically observed in Figure 3. As a consequence, despite the significant bias compared to reference values, Logan can be considered the most robust of the three methods for the generation of parametric V_T images, showing a higher precision independent of receptor density levels.

Parametric images of receptor binding were also comparable between different parametric methods. Moreover, a good correspondence to VOI-counterparts was seen for all reference methods, with high R^2 values and only small over- and underestimations seen for RPM and SRTM2, respectively (Table 3). In comparison with reference 2TCM values, correlation remained high for all methods, and linear regression slopes were closer to the identity line for the SRTM2. However, RLogan consistently underestimated binding, with a regression slope of 0.86. Interestingly, while RPM and SRTM2 had overall bias similar to those of RLogan (-0.10, 0.05 and -0.17, respectively), the range of differences to 2TCM values was larger for those methods (Figure 3). In fact, the differences seen between SRTM2 and 2TCM estimates reached 0.5 for regions of low-binding – values higher than the actual BP_{ND} estimates,

translating into relative errors of more than 100% (Figure 4B and 4C). However, those correspond to BP_{ND} values close to zero, where large relative errors are not surprising, nor meaningful. On the other hand, It is also important to notice that all reference based methods underestimate the true BP_{ND} from the start, due to the considerable levels of specific binding present in the rat pons[16]. Nonetheless, RLogan displayed the highest precision in estimating receptor binding, as can be seen in Figure 3. Therefore, despite its bias to 2TCM values, RLogan can be considered the most robust reference based parametric method for the generation of receptor binding images.

While V_T and BP_{ND} are important kinetic parameters, both require dynamic scanning for their estimation. As a consequence, SUV and SUVR determined from static late images are widely applied for both regional and parametric analyses. While SUV does not necessarily correspond to V_T, both parameters are directly related. This was also seen in our findings, where good correlation (R^2>0.95) was found between parametric SUV determined at three p.i. intervals and 2TCM V_T (Figure 5A). In turn, SUVR is closely related to BP_{ND}, and when equilibrium is reached, SUVR – 1 is expected to correspond to DVR – 1. Therefore, a more direct comparison between SUVR – 1 from different intervals p.i. and BP_{ND} could be performed. However, as can be seen in Figure 1, this method overestimated BP_{ND} from other methods, as well as DVR – 1 from 2TCM (Table 3). The largest overestimation of 2TCM DVR – 1 was seen for $SUVR_{40\text{-}50}$, and the smallest for $SUVR_{50\text{-}60}$, which might indicate equilibrium is not reached at earlier intervals. Nonetheless, all SUVR – 1 strongly correlated to 2TCM DVR – 1. It is important to notice that despite the high correlations, the performance of SUV and SUVR – 1 was region-dependent (Figure 5A and 6A, respectively). However, when assessing agreement by a ratio Bland-Altman, the results suggested a scaling effect for SUV, since relative errors were similar across regions (Figure 5B). Although useful, SUV and SUVR images must be applied carefully in group comparisons and longitudinal studies, since they are especially affected by changes in metabolism and tissue perfusion [22].

In summary, the results of this study indicate that parametric analysis of [^{11}C]flumazenil images of the rat brain can be satisfactorily performed. As a consequence, parametric imaging and statistical parametric mapping (SPM) analysis would allow direct statistical comparison

across groups and/or conditions without prior assumptions on regions of interest. In fact, SPM analysis has previously been able to detect more subtle disease-related changes in an animal model of inflammation, for example[23]. However, the homogeneous dataset analyzed in this study did now allow for a similar assessment of the performance of parametric imaging in group comparison, nor was this within the scope of the study. Thus, further studies should be performed in order to evaluate the benefit of parametric imaging of [^{11}C]flumazenil binding in the rat brain for different conditions and study designs.

While all methods showed good performance, different methods might be better suited for specific applications and study designs. In that context, since Logan and RLogan outperformed other methods in precision and are of robust and simple implementation, both methods are preferred for group comparisons and longitudinal studies. However, these methods do not produce additional quantitative metrics such as K_1 or R_1. In that sense, alternatives such as BFM or RPM can be of value in generating parametric images with additional information, while maintaining good correlation between their primary endpoints and 2TCM values. On the other hand, all of the methods mentioned above require dynamic scanning, and might therefore pose a challenge for some study designs. In such cases, SUV and SUVR images could be useful despite under- and overestimation of kinetic parameters, since high correlation values were found in comparison to 2TCM values. However, these static parameters must be considered carefully when possible changes in metabolism or perfusion cannot be excluded, in particular in the case of displacement, interventional or longitudinal studies.

Conclusion

This study demonstrated several parametric methods performed well for the generation of [^{11}C]flumazenil distribution and binding images. Good correlation to 2TCM derived values was observed across all methods, and therefore, a specific method should be applied according to what information is of interest to a specific research question. Nonetheless, the most precise and straightforward methods were found to be Logan and RLogan, while BFM or RPM could be considered when information on perfusion is of significance.

REFERENCES

1. Heiss, W. D. *et al.* Permanent cortical damage detected by flumazenil positron emission tomography in acute stroke. *Stroke.* **29,** 454–61 (1998).
2. Heiss, W. D. *et al.* Early [(11)C]Flumazenil/H(2)O positron emission tomography predicts irreversible ischemic cortical damage in stroke patients receiving acute thrombolytic therapy. *Stroke.* **31,** 366–9 (2000).
3. Tian, J., Yong, J., Dang, H. & Kaufman, D. L. Oral GABA treatment downregulates inflammatory responses in a mouse model of rheumatoid arthritis. *Autoimmunity* **44,** 465–70 (2011).
4. Heiss, W. D. *et al.* Probability of cortical infarction predicted by flumazenil binding and diffusion-weighted imaging signal intensity: A comparative positron emission tomography/magnetic resonance imaging study in early ischemic stroke. *Stroke* **35,** 1892–1898 (2004).
5. Rojas, S. *et al.* Positron emission tomography with 11C-flumazenil in the rat shows preservation of binding sites during the acute phase after 2h-transient focal ischemia. *Neuroscience* **182,** 208–216 (2011).
6. Wong, C. G. T., Bottiglieri, T. & Snead, O. C. GABA, gamma-hydroxybutyric acid, and neurological disease. *Ann. Neurol.* **54 Suppl 6,** S3-12 (2003).
7. Barragan, A., Weidner, J. M., Jin, Z., Korpi, E. R. & Birnir, B. GABAergic signalling in the immune system. *Acta Physiol. (Oxf).* **213,** 819–827 (2015).
8. Innis, R. B. *et al.* Consensus Nomenclature for in vivo Imaging of Reversibly Binding Radioligands. *J. Cereb. Blood Flow Metab.* **27,** 1533–1539 (2007).
9. Gunn, R. N., Gunn, S. R. & Cunningham, V. J. Positron Emission Tomography Compartmental Models. *J. Cereb. Blood Flow Metab.* **21,** 635–652 (2001).
10. Lammertsma, a a & Hume, S. P. Simplified reference tissue model for PET receptor studies. *Neuroimage* **4,** 153–8 (1996).
11. Koeppe, R. a, Holthoff, V. a, Frey, K. a, Kilbourn, M. R. & Kuhl, D. E. Compartmental analysis of [11C]flumazenil kinetics for the estimation of ligand transport rate and receptor distribution using positron emission tomography. *J. Cereb. Blood Flow Metab.* **11,** 735–44 (1991).
12. Geeraerts, T. *et al.* Validation of reference tissue modelling for [11C]flumazenil positron emission tomography following head injury. *Ann. Nucl. Med.* **25,** 396–405 (2011).
13. Klumpers, U. M. *et al.* Comparison of Plasma Input and Reference Tissue Models for Analysing [11 C]flumazenil Studies. *J. Cereb. Blood Flow Metab.* **28,** 579–587 (2008).
14. Salmi, E. *et al.* Measurement of GABAA receptor binding in vivo with [11C]flumazenil: a test-retest study in healthy subjects. *Neuroimage* **41,** 260–9 (2008).
15. Klumpers, U. M. H. *et al.* Parametric [11C]flumazenil images. *Nucl. Med. Commun.* **33,** 422–30 (2012).
16. Lopes Alves, I., Vállez García, D., Parente, A., Doorduin, Lopes Alves, I., Vállez García, D., Parente, A., Doorduin, J., Marques da Silva, A., Koole, M., Willemsen, A. T. M., Dierckx, R., Boellaard, R. [11C]flumazenil kinetics in the rat brain: model preference and the impact of non-specific and non-selective binding in reference region modeling. *Eur. J. Nucl. Med. Mol. Imaging* **43,** S25 (2016).
17. Vállez Garcia, D. *et al.* A standardized method for the construction of tracer specific PET

and SPECT rat brain templates: validation and implementation of a toolbox. *PLoS One* **10,** e0122363 (2015).
18. Boellaard, R., Yaqub, M., Lubberink, M. & Lammertsma, A. PPET: A software tool for kinetic and parametric analyses of dynamic PET studies. *Neuroimage* **31,** T62 (2006).
19. Cunningham, V. J. & Jones, T. Spectral Analysis of Dynamic PET Studies. *J. Cereb. Blood Flow Metab.* **13,** 15–23 (1993).
20. Gunn, R. N., Lammertsma, A. A., Hume, S. P. & Cunningham, V. J. Parametric imaging of ligand-receptor binding in PET using a simplified reference region model. *Neuroimage* **6,** 279–87 (1997).
21. Wu, Y. & Carson, R. E. Noise reduction in the simplified reference tissue model for neuroreceptor functional imaging. *J. Cereb. Blood Flow Metab.* **22,** 1440–1452 (2002).
22. van Berckel, B. N. M. *et al.* Longitudinal amyloid imaging using 11C-PiB: methodologic considerations. *J. Nucl. Med.* **54,** 1570–1576 (2013).
23. Parente, A. *et al.* Pharmacokinetic Analysis of 11C-PBR28 in the Rat Model of Herpes Encephalitis: Comparison with (R)-11C-PK11195. *J. Nucl. Med.* **57,** 785–791 (2016).

Overview and discussion